New Methodology to Evaluate the Rolling Contact Fatigue Performance of Bearing Steels With Surface Dents: Application to 32CrMoV13 Nitrided and M50 Steels

Daniel Nelias, Christophe Jacq, Gérard Lormand, G. Dudragne, Alain Vincent

New Methodology to Evaluate the Rolling Contact Fatigue Performance of Bearing Steels With Surface Dents: Application to 32CrMoV13 Nitrided and M50 Steels

D. Nélias, LaMCoS, UMR CNRS 5514, INSA Lyon, France
C. Jacq, SNECMA Moteurs, Villaroche, France
G. Lormand, GEMPPM, UMR CNRS 5510, INSA Lyon, France
G. Dudragne, SNR Bearings, Annecy, France
A. Vincent, GEMPPM, UMR CNRS 5510, INSA Lyon, France

A new methodology is proposed to evaluate the rolling contact fatigue (RCF) perfor-mance of bearing steels in presence of surface dents. The experimental procedure con-sists of denting the raceway of test specimens with a hardness machine using spherical diamond tips of different radii (i.e., 200, 400, and 600m) and with an applied normal load ranging from 5 to 50daN. Analysis of various dent geometries yield an analytical law with five parameters useful for fitting experimental profiles for contact simulation. Fatigue tests are conducted using a two-disk machine to study the effect of different operating conditions on RCF and to compare the performances of nitrided 32CrMoV13 steel versus M50 reference steel. A numerical investigation is conducted to analyze ex-perimental result. Initially, the local residual stresses and plastic strains around the dent are obtained through finite element simulations of the indentation process. Second, the overrolling of the dent is simulated with a contact code. Finally, an indent-based endur-ance limit, called H1I, is proposed and comparisons are made with test results. Both RCF tests and numerical simulations show improved performance with nitrided 32CrMoV13 steel when compared to the M50 reference steel. The dominating role of sliding is also experimentally highlighted and two areas of damage initiation are identified. The effects of normal load and hoop stress are less marked.

Introduction

Rolling contact fatigue (RCF) is a major cause of rolling bearing failure [1]. Because of the repeated contact between rolling elements, RCF is accelerated considerably when surface defects, such as dents, exist on the surface of the contacting bodies [2]. Dents created by hard solid particles suspended in the lubricant cannot be totally removed since perfect filters or seals do not exist. Therefore, rolling element bearings should be designed to endure surface dents.

Nitrided steels have shown promise as potential material for rolling element bearings [3] and seem particularly resistant to raceway damage, such as dents. The benefits provided by surface nitriding highly loaded components arises from the combination of high surface hardness due to the nitrided surface layer and a high core toughness. The nitriding treatment hardens the material surface up to the Hertzian depth and introduces compressive residual stresses in the nitrided layer [4]. These are known to be beneficial for RCF. Therefore, nitrided 32CrMoV13 steel (AMS 6481) was found to be a good candidate.

Ko and Ioannides [5] were the first to perform an elastic-plastic analysis of the subsurface stress state due to debris denting. In their analysis, using the finite element method (FEM), the contact problem was not solved and a given pressure distribution was considered, hence, neglecting the effect of plastic strain and subsequent hardening due to indentation. More recently Sadeghi and co-workers have performed advanced numerical simulations by FEM [6–10]. The problem of a rolling load over a surface defect was first investigated in 1996 [6], again without plastic strain and residual stress due to indentation. Later Xu et al. studied the indentation of a thru-hardened steel by a rigid spherical tip and subsequent overrolling of the dent [7,8]. Zhao et al. analyzed the effect of a dent in a line contact [9] considering the fluid entrapment in the dent pocket. More recently Kang et al. [10] determined the shape of a soft debris while traveling through the contact conjunction. Unfortunately the computational cost of such a simulation did not allow the use of a fine mesh, required to predict the plastic strain and residual stress in the vicinity of the dent. However, the macrogeometry of the dent (i.e., depth and diameter) was obtained in their study. Howell et al. [11] performed a finite element simulation of rolling contact over four differently sized spherical dents. The effect of dent size on the pressure distribution and fatigue failure location was studied for 52100 bearing steel. In their analysis the material model used was adjusted to match both the stress amplitude versus strain range curve and experimental ratchetting.

To the author's knowledge the literature does not provide quantitative data about the effects of operating conditions on rolling contact fatigue and little is known about the damage mechanisms of surface-hardened steels in presence of surface stress raisers. Therefore, the aim of the present work is (i) to evaluate the RCF performance of nitrided 32CrMoV13 steel versus M50 (AMS 6490) aerospace baseline steel, both with artificially induced dents; (ii) to quantify the influence of the Hertz pressure, slide-to-roll ratio, and hoop stresses on RCF; and (iii) to identify damage initiation sites.

The experimental investigation was performed on a high-speed two-disk machine with operating conditions representative of

Table 1 Chemical composition of nitride 32CrMoV13 steel

C	Si	Mn	Ni	Cr	Mo	V
0.334	0.24	0.48	0.10	2.93	0.9	0.32

those encountered in a commercial turbine engine main-shaft roller bearing. Geometry and loading conditions were carefully chosen to reproduce the contact stress profile encountered in the above application, especially with regard to the microyield shear stress profile determined by Jacq et al. [12]. A simple and discriminating procedure is proposed. It consists of denting the raceway of the test specimen with a hardness machine using different diamond tips (i.e., 200, 400, and 600 μm radius) and normal loads ranging from 5 to 50 daN. Simulation of denting by the FEM was performed to determine the proper dent geometry and residual stress state around the surface defect. This, along with the knowledge of the microyield stress profile obtained by nanoindentation, was necessary for the three-dimensional (3D) cyclic elastic-plastic analysis.

Experimental Procedure

Material. The chemical composition of the 32CrMoV13 steel studied here is given in Table 1. Before nitriding at 550°C, specimens were austenised at 950°C for 20 min, quenched in oil and then annealed at 630°C for 3 h. The compound layer, which formed at the surface of the material during nitriding, was removed by grinding. The penetration depth of nitrogen obtained after this treatment is ~600 μm.

Two-Disk Machine and Operating Conditions. Fatigue tests were performed using a high-speed twin-disk machine [13] whose principle is briefly recalled below. Two spherical rotating disks are brought in contact with an imposed load. The rotating speed of disks is controlled independently, hence enabling various contact conditions, such as pure rolling or controlled sliding. Since nitrided 32CrMoV13 steel is surface hardened, the loading condition must account for, not only the Hertzian stress profile, but also the residual stress versus depth profile inherent to the nitriding process, which is then subsequently compared to the microyield shear stress profile. This problem has been stated by Vincent et al. [14], who described the variation of the RCF endurance limit $H1$ for a spherical point contact as a function of the contact equivalent radius of curvature in the case of nitrided 32CrMoV13 steel. Subsequently, special care has been taken in setting the operating conditions so that the stress profile obtained in the experimental test disk (labeled TD in Fig. 1) is close to that encountered in the application, i.e., a typical aeronautical rolling bearing (ARB) (labeled ARB in Fig. 1). This consideration has led to the selection of an equivalent radius of 15 mm, obtained with a disk specimen (dented) of 24 mm radius and an opposite disk (smooth) of

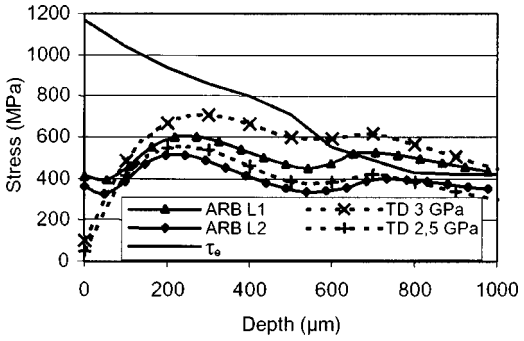

Fig. 1 Von Mises and microyield shear stress profiles

Table 2 Fatigue tests operating conditions

Label	Specimen	Contact Stress (GPa)	Sliding	Hoop stress (MPa)
C1	M50	2.5	0	0
C2	M50	3	1.5 %	0
ES1	Nitrided	2.5	0	0
ES2	Nitrided	2.5	0	115
ES3	Nitrided	2.5	1.5 %	0
ES4	Nitrided	2.5	1.5 %	115
ES5	Nitrided	3	0	0
ES6	Nitrided	3	0	115
ES7	Nitrided	3	1.5 %	0
ES8	Nitrided	3	1.5 %	115

40 mm radius. Two loads are considered, 2.5 and 3 GPa. The resulting radius of the contact zone is 510 and 610 μm, respectively. Nitrided 32CrMoV13 steel specimen disks were tested against M50 disks, since in the bearing application, M50 rollers are used with nitrided 32CrMoV13 rings. For comparison, tests were also conducted on all-M50 disk specimens. MIL-L-23699-type turbine engine oil was used as the lubricant and delivered to the contact at 80°C. The linear velocity at the contact was 24 m s^{-1}. To investigate the effect of sliding, tests were carried out under pure rolling conditions and with a slide-to-roll ratio of 1.5%. It should be noted that in order to achieve sliding, the nitrided disk velocity was lowered. Lastly, the effect of tensile hoop stress was investigated by superimposing a 115 MPa interference fit on some of the nitrided disks by press fitting. The operating conditions are summarized in Table 2.

Indentation Procedure. Artificially controlled dents were made with spherical diamond indenters of different radii R_p (R_p =200, 400, and 600 μm) and at various loads W_i (W_i =5,10,20,30,50 daN). All dents were made on the 24 mm radius disk. These are identified by the radius of the indenter and by the applied load. Hence, dent 200-20 corresponds to a dent made with R_p=200 μm under a load W_i=20 daN. The geometrical characteristics of dents thus obtained (diameter ϕ, depth h_p, and shoulder height h_b, Fig. 2) are summarized in Table 3. Up to 18 dents have been tested simultaneously on each specimen.

Results

Damage Criterion. An objective of the experiments was to determine whether a given dent was harmful or not; that is, if microspalls appeared around the dent, then it was considered harmful. To determine this, two tests, C1 and C2, were run for 40 and 50×10^6 cycles. All damage visible at the end of these two tests were initiated before 20×10^6 cycles. For example, the dent 200-10 in Fig. 3, which did not exhibit microspalls after 10 million cycles (Fig. 3(a)), remained optically identical up to 50 million cycles. Therefore, a dent was considered harmful for a given operating condition if microspalls appeared around the dent

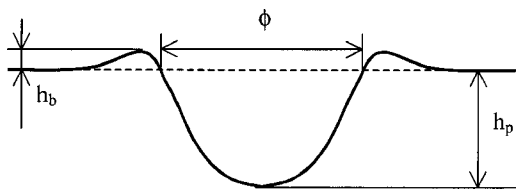

Fig. 2 Dent geometry

Table 3 Measured values of the dent geometry parameters

32CrMoV13 (nitrided)									
Indentation		Dent			Indentation		Dent		
Radius (μm)	Load (daN)	ϕ (μm)	h_p (μm)	h_b (μm)	Radius (μm)	Load (daN)	ϕ (μm)	h_p (μm)	h_b (μm)
200	5	85	3.5	0.4	400	20	180	6.5	0.6
200	10	120	6	0.7	400	30	210	10	0.8
200	20	170	13	1.4	400	50	290	18	0.9
200	30	200	20	2.7	600	20	195	4	0.3
200	50	260	32	4	600	30	225	6	0.3
400	10	125	2.5	0.6	600	50	290	11	0.7
M50									
Indentation		Dent			Indentation		Dent		
Radius (μm)	Load (daN)	ϕ (μm)	h_p (μm)	h_b (μm)	Radius (μm)	Load (daN)	ϕ (μm)	h_p (μm)	h_b (μm)
200	5	90	3.5	0.3	400	20	190	7.5	0.3
200	10	130	7	0.4	400	30	220	11	0.4
200	20	170	14	1.3	400	50	280	18	0.6
200	30				600	20	190	4.5	0.5
200	50				600	30	230	7	0.6
400	10	140	3	0.2	600	50	300	12	0.7

at 20×10^6 fatigue cycles. It should be emphasized that this strict criteria is focused on the occurrence of localized surface damage and not on its evolution to generalized micropitting or deep spalling.

Test Summary. The results are summarized in a visual manner in Table 4. Each cell corresponds to the mean behavior of several identical dents (at least three on at least two different disks). Each column corresponds to an indentation load W_i and each row to an indenter radius R_p. When at least one of the dents is responsible for damage, the type of dent is then considered harmful for the given operating condition and the cell is shaded. Cells are left blank when no damage is observed (for all identical dents) as well as for cells on the same line on the left-hand side (i.e., for lower indentation loads and for those not tested). Cells with question marks indicate the dent has not been tested, and the boundary between harmful and harmless remains undetermined.

Nitrided 32CrMoV13 Versus M50. The operating conditions C2 and *ES*7 correspond to tests at 3 GPa, 1.5% sliding, and with no hoop stress added. The C2 condition corresponds to dented M50 disks, whereas the *ES*7 corresponds to dented nitrided 32CrMoV13 disks. The results given in Table 4 (C2 versus *ES*7) show that dents 400-20, 600-20, and 600-30 can be classified as harmful for M50 but not for nitrided 32CrMoV13. Hence, when compared to M50, the nitrided steel exhibits improved fatigue strength as far as dent initiated RCF is concerned.

Effect of Sliding. When 1.5% sliding is introduced, 15 cells change status when compared to results obtained under pure rolling conditions (*ES*1/*ES*3, *ES*2/*ES*4, *ES*5/*ES*7, *ES*6/*ES*8). For each operating condition, the dents 400-30, 400-50, and 600-50 become harmful when sliding is introduced. Dent 400-20 also becomes harmful when combined with hoop stress. These results indicate that sliding has a major detrimental effect on dent initiated RCF. Therefore, dent initiated RCF can become more severe in applications where even low levels of sliding are present.

Effect of Hoop Stress. When a 115 MPa hoop stress is introduced (*ES*1/*ES*2, *ES*3/*ES*4, *ES*5/*ES*6, and *ES*7/*ES*8), three cells change status (dent 400-20 in *ES*3-4 and dents 400-20 and 600-30 in *ES*7-8). These results suggest that the presence of hoop stress tends to degrade dent-initiated RCF resistance. However, this effect is limited to the given operating conditions. As for the contact load, the hoop stress may be a very important parameter for the growth of nucleated damage to deep spalling.

Effect of Normal Load. When the load increases from 2.5 to 3 GPa (*ES*1/*ES*5, *ES*2/*ES*6, *ES*3/*ES*7, and *ES*4/*ES*8), only one cell changes status (dent 600-30 from *ES*4 to *ES*8). However, in this case, no change was observed in dent behavior while increasing the load. This result implies that the given load increase has little influence on dent-initiated RCF. It should be

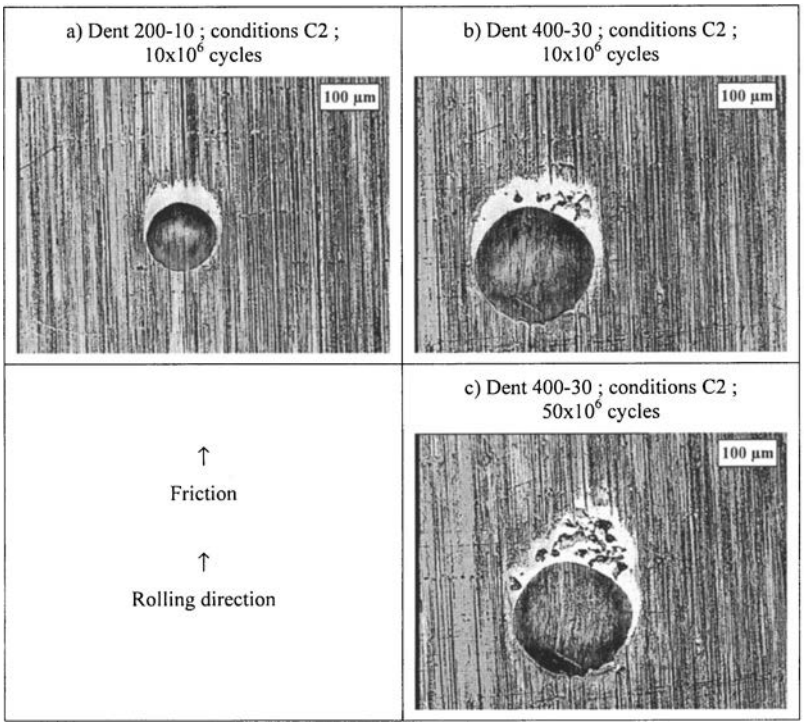

Fig. 3 Dent 200-10 and 400-30 at 10×10^6 and 50×10^6 cycles. Operating conditions C2 (M50 disks).

Table 4 Experimental results for conditions *C*2 and *EI*1 to *ES*8

C2	3 daN	5 daN	10 daN	20 daN	30 daN	50 daN
200 μm	???	???				
400 μm						
600 μm	???	???	???			

ES1	3 daN	5 daN	10 daN	20 daN	30 daN	50 daN
200 μm						
400 μm						???
600 μm						

ES2	3 daN	5 daN	10 daN	20 daN	30 daN	50 daN
200 μm						
400 μm						???
600 μm						

ES3	3 daN	5 daN	10 daN	20 daN	30 daN	50 daN
200 μm						
400 μm						
600 μm						

ES4	3 daN	5 daN	10 daN	20 daN	30 daN	50 daN
200 μm						
400 μm						
600 μm						

ES5	3 daN	5 daN	10 daN	20 daN	30 daN	50 daN
200 μm						
400 μm						???
600 μm						

ES6	3 daN	5 daN	10 daN	20 daN	30 daN	50 daN
200 μm						
400 μm						???
600 μm						

ES7	3 daN	5 daN	10 daN	20 daN	30 daN	50 daN
200 μm						
400 μm						
600 μm						

ES8	3 daN	5 daN	10 daN	20 daN	30 daN	50 daN
200 μm						
400 μm						
600 μm						

mentioned that this conclusion is valid only for the load range encountered in aeronautical bearings (2–3 GPa). At higher loads, other phenomena might be activated and, conversely, no damage is likely to occur in the very low load range. This conclusion must be restricted to the nucleation of damage, since the growth stage leading to deep spalling might be more dependent on the load rather than the initiation stage because the growth stage requires a stress high enough at Hertzian depth.

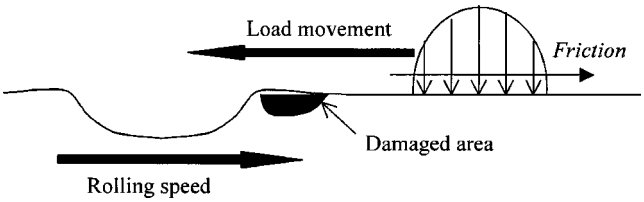

Fig. 4 Location of the damaged area for driven surface in presence of sliding

Location of Surface Damage. The location of the damaged area for each dent tested under pure rolling conditions was always ahead of the dent, along the direction of load movement (Fig. 4). The same phenomenon was observed with dents tested with sliding, however, the damage was more pronounced here than under pure rolling conditions. These observations are consistent with transient elastohydrodynamic lubrication (EHL) analysis, which predicts a slightly higher pressure peak ahead of the dent, along the load movement direction under pure rolling and a more significant peak when sliding is present for dents located on the slower surface [15]. Note that the detrimental effect of sliding may also be explained by a possible cavitation phenomenon and subsequent localized microcollapse of the lubricant film [16].

A typical damage found in the vicinity of a 200-20 dent is shown in Figs. 5(*a*) and 5(*b*) for pure rolling and rolling plus sliding conditions, respectively. It may be noted that the dent edge is jagged for pure rolling, whereas it remains smooth and circular for the condition with 1.5% sliding. Moreover, microspalls that appear close to the dent edge are always located away from the border.

Finally, two areas of damage nucleation have been identified. The first, called RIZ (rolling initiation zone) as shown in Fig. 6, is activated only under pure rolling conditions and corresponds to the dent edge. Its position is given in the present experiment by the rolling direction of the dented surface. The second area, denoted FRIZ (friction and rolling initiation zone), is located at about 20 μm ahead of the dent along the friction direction.

Analysis

RCF Results From Repeated Overrolling. The analysis of the fatigue process requires the knowledge of material properties and loading conditions during initial denting and further overrolling. These properties include (i) the microyield shear stress profile, required for defining the endurance limit; (ii) the hardening law of the material, necessary to describe the indentation process that involves plasticity; and (iii) the residual stresses induced by the nitriding treatment. These contribute to stresses in the material from the indentation and overrolling process.

The microyield shear stress and uniaxial hardening behavior are usually measured by bulk compressive tests made on material samples. This process gives average values over the section of the sample. Therefore, to be relevant, this test must be made on homogeneous samples. Toward this end, two types of homogeneous sample (*A* and *B*) were tested. The first type, *A*, of cylindrical shape, is made of nitrided 32CrMoV13 from which the nitrided layer was totally removed to represent the core material. The second type, *B*, was obtained by homogeneously nitriding thin tubes of 32CrMoV13 steel [3]. It represents the behavior of a quasi-uniform nitrided layer. Results obtained from these two tests are plotted in Fig. 7. Two conclusions arise from these tests. First, the plastic behavior can be represented by the Swift law [$\sigma = B(C + 10^6 \times \varepsilon^p)^n$] [3], where B, C, and n are three parameters of the law. This law describes the uniaxial hardening and gives the microyield shear stress τ_e[$2\tau_e = B(C+20)^n$]. Second, both tests can be described with identical C and n parameters, here equal to 16

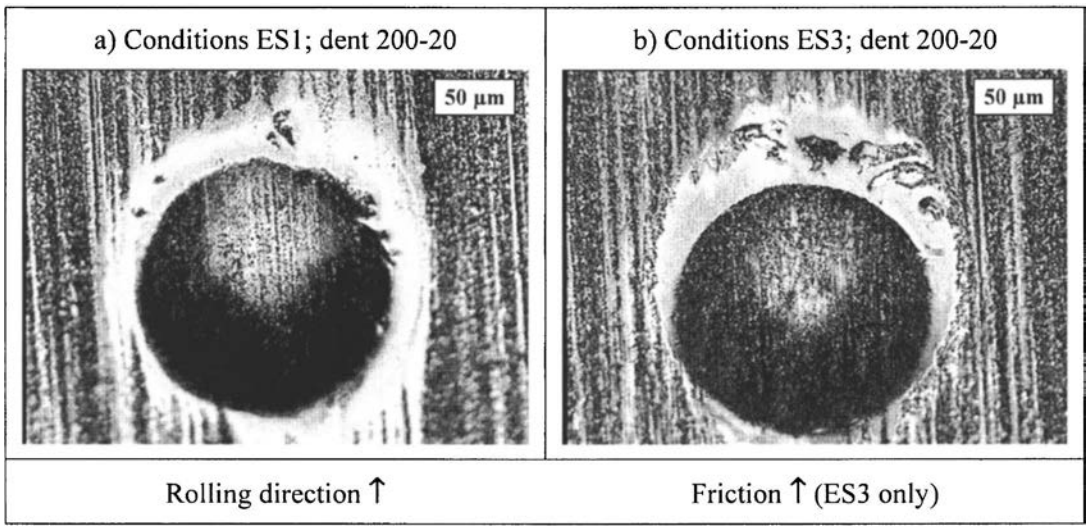

Fig. 5 Dent 200-20 at 20×10^6 cycles; effect of sliding (Nitrided 32CrMoV13)

and 0.067, respectively. In conclusion, the variation of the mechanical behavior in the nitrided layer can be described by the variation of B.

The dent shape can be determined by simple topographical measurements, however, local residual stresses and hardening state of the material are not readily available from measurement. It is then necessary to simulate the indentation process to estimate the material state. To attest the quality of such an estimation, the first step is to compare the real geometry of the dent with that obtained by simulation. The result will depend on the shape and material of the indenter tip, the normal load applied during indentation, and the elastic-plastic properties of the dented material.

Indenter heads have a conical shape with a cone angle of 120 deg. Their extremity is made of a spherical diamond tip ($E=1140$ GPa, $\upsilon=0.07$) with a radius R_p of 200, 400, or 600 μm. The applied normal load during indentation W_i is chosen between

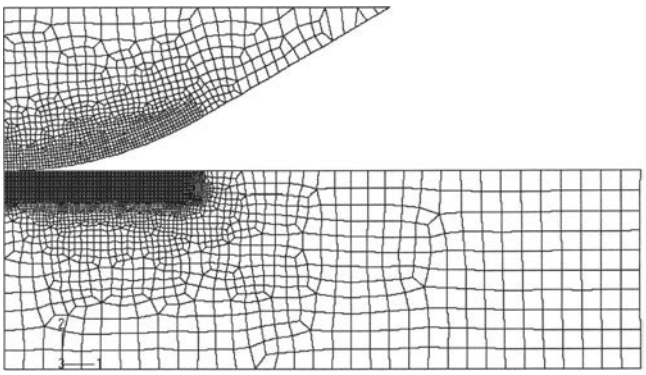

Fig. 8 FE mesh used for indentation simulation

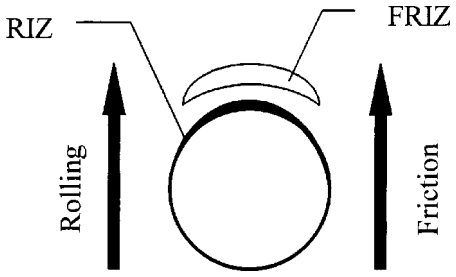

Fig. 6 Location of damaged areas: rolling initiation zone (RIZ) and friction and rolling initiation zone (FRIZ)

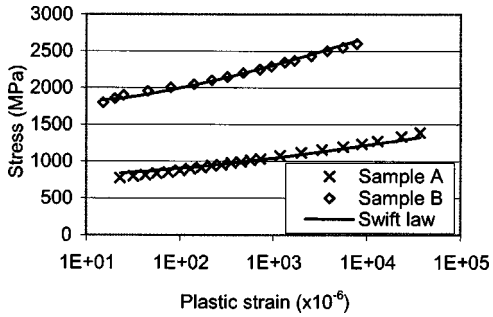

Fig. 7 Stress-plastic strain curve for samples *A* and *B*

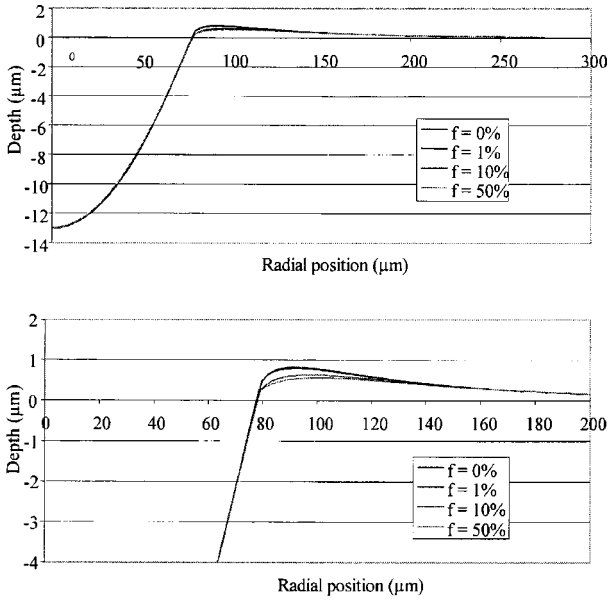

Fig. 9 Influence of friction on the dent shape (dent 200-20, M50). Coefficient of friction f=0, 1, 10, and 50%; (*a*) General view and (*b*) zoom on the dent shoulder.

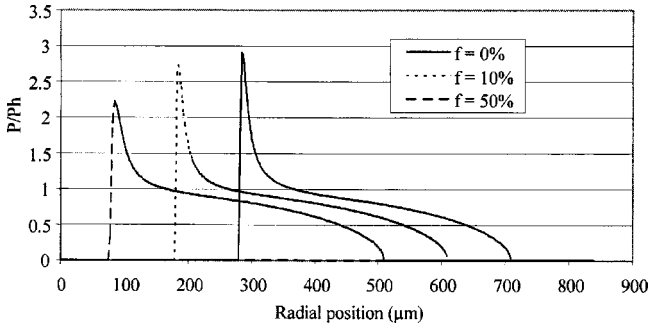

Fig. 10 Influence of friction coefficient *f* during indentation on contact pressure *P* normalized by the Hertz pressure P_H (dent 200-20, M50). For clarification, the profiles *f*=10% and *f*=50% are shifted along the radial axis.

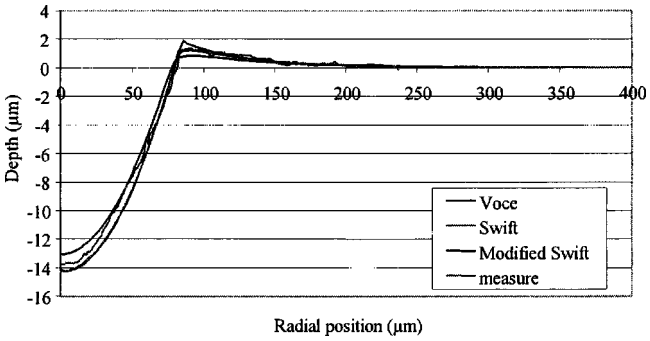

Fig. 12 Influence of the extrapolated hardening law on the dent shape for M50: dent 200-20, *f*=0%

5, 10, 20, or 50 daN. The friction coefficient between the indenter head and the material to be dented is unknown during the indentation step. Therefore, the first step is to analyze the effect of friction coefficient on the dent shape.

The elastic-plastic properties of bearing steels, such as AISI 52100, M50, and nitrided 32CrMoV13, are only known within plastic strains of up to 2%. However, plastic strain can reach up to 40% during some Rockwell indentations [17]. Therefore an extrapolation of the hardening law is required and should be experimentally validated.

Indentation Simulation. The indentation process was simulated using the ABAQUS commercial FE code. The problem is axisymmetric since the punch and the facing body have a common axis of revolution. The mesh used for this simulation is presented in Fig. 8. The mesh size is 2 μm in the contact zone, which is small when compared to the dent diameter (150–300 μm). The body is meshed with 5050 nodes, and the punch is described by 1000–1700 nodes, depending on its radius.

An isotropic plasticity model is used to describe the behavior of the body being dented (M50 or nitrided 32CrMoV13). The punch behavior is assumed purely elastic (diamond). The load is applied by a uniform pressure on the upper surface of the punch, whose nodes are unable to move radially. Boundary conditions are applied through half-infinite elements in order to simulate the half-space body. The problem should be solved with large strains. Therefore, the hardening law is expressed in terms of the Cauchy stress versus the logarithmic strain.

First, the effect of the friction coefficient between the punch and the specimen is investigated. Results are presented in Fig. 9 for M50 material and dent 200-20. Figure 9(*b*) shows that the dent shoulder height decreases significantly from 0.8 to 0.6 μm when the friction coefficient increases to 0.5, whereas the location of the shoulder top moves radially from 90 to 100 μm. In contrast, the dent depth and its radius are almost independent of the friction coefficient (Fig. 9(*a*)).

To evaluate the effect of these geometrical changes, the elastic contact between two spheres of equivalent radius, R_{eq}=15 mm, was solved for dents simulated with a friction coefficient equal to 0, 0.1, and 0.5 (shape given in Fig. 9). The resulting pressure profiles are given in Fig. 10 in dimensionless form (by P_H, the Hertz pressure). A marked decrease in the peak pressure is observed, going from 2.9 to 2.2 P_H when the friction coefficient increases from 0 to 0.5. Since the indentation procedure is a slow process made in the presence of traces of lubricant (boundary lubrication), a friction coefficient of 0.1 is assumed from here on.

Extrapolation of the Hardening Law. As stated above, elastic-plastic properties of bearing steels are known from uniaxial compression tests only up to 1 or 2% of plastic strain. An estimate of the hardening law is proposed below for both M50 and nitrided 32CrMoV13 steel based on the real geometry of dent 200-20.

M50. The elastic-plastic behavior of M50 could be described up to 2% of plastic strain by the Swift law, $\sigma_{eq}=B(C+10^6\times\varepsilon_p)^n$, with B=1280 MPa, C=4, and n=0.095. Three different extrapolations of the hardening law, as described below, are plotted in Fig. 11:

- The Swift law, which originally identified up to 2% plastic strain, is simply extended up to 40%.
- The modified Swift law, which is the direct transposition of the Swift law in true stress and logarithmic strain. The gap with the Swift law appears only beyond 2% plastic strain.
- The Voce law, which presents a horizontal asymptote rather than a continuous increase as with the Swift law. This law was successfully used by Cercueil [17] for indentation of AISI 52100 steel. The four parameters of this law were cho-

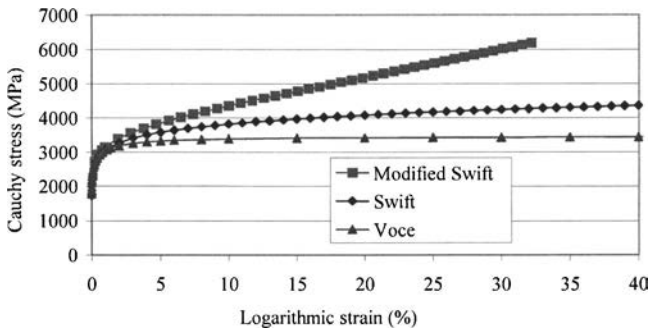

Fig. 11 Possible extrapolations of M50 hardening laws

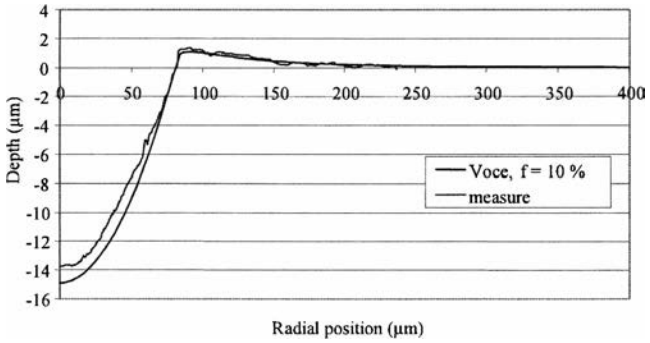

Fig. 13 Comparison between measured and simulated 200-20 dent profiles: M50 steel, Voce law, *f*=10%

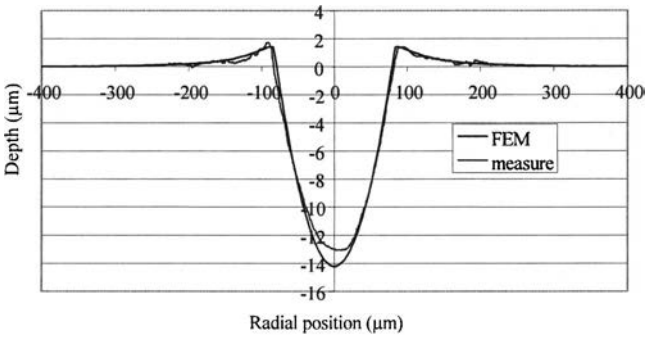

Fig. 14 Comparison between measured and simulated 200-20 dent profiles: 32CrMoV13 steel, Voce law, f=10%

sen to give a similar curve as the Swift law in the domain 0–2% plastic strain

$$\sigma_{eq} = 1444 + 1996\{1 - \exp[-(390 \times \varepsilon_p)^{0.352}]\} \text{ (in MPa)} \quad (1)$$

Figure 12 shows the result of simulations performed without friction using these three laws, as well as one real profile measured from dent 200-20 on M50 steel. The height of the dent's shoulder obtained with the modified Swift law is too small when compared to the measurement. Nonetheless, the result obtained with the Swift law is more important at this point. It should be noted that since the friction coefficient was not introduced in this simulation, it overestimates the shoulder height. Thus, a shoulder height significantly less than the measured value would have resulted with friction. Finally, the Voce law, which results in the highest shoulder in Fig. 12 (f=0%), gives a very satisfactory result in presence of friction (10%), especially in the vicinity of the shoulder as shown in Fig. 13.

Nitrided 32CrMoV13. In the present study, the mechanical properties of the nitrided material can be assumed homogeneous within the scale of the dent's influence zone ($<$150 μm) since it is small in comparison to the nitrided depth (600–800 μm). Similarly to M50 steel, the Voce law gave

$$\sigma_{eq} = 1930 + 1380\{1 - \exp[-(455 \times \varepsilon_p)^{0.490}]\} \text{ (in MPa)} \quad (2)$$

Good agreement is shown in Fig. 14 between simulation and measurement profiles for dent 200-20 on nitrided 32CrMoV13 steel, particularly around the dent shoulder, which is of prime interest for contact problems. It should be noted that the initial residual stress due to the nitriding treatment was considered (i.e., −400 MPa in the stressed zone).

Figure 15 shows that good correlation is obtained with dents produced by punches of radius 400 and 600 μm using Eqs. (1) and (2) for both M50 and nitrided 32CrMoV13 steels, respectively.

Residual Plastic Strain. The accumulated plastic strain (in percent) introduced during indentation is given in Fig. 16. The depth

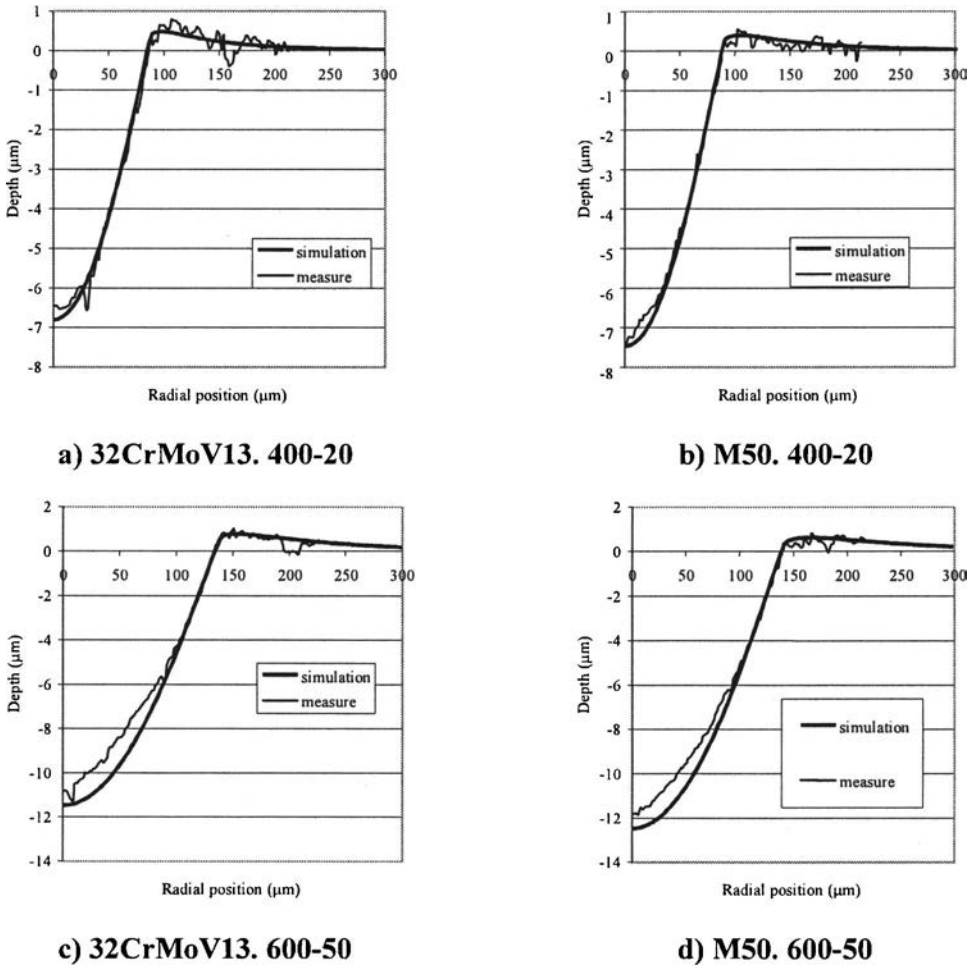

Fig. 15 Comparison of measured and simulated dent profiles for dents 400-20 and 600-50 on 32CrMoV13 and M50

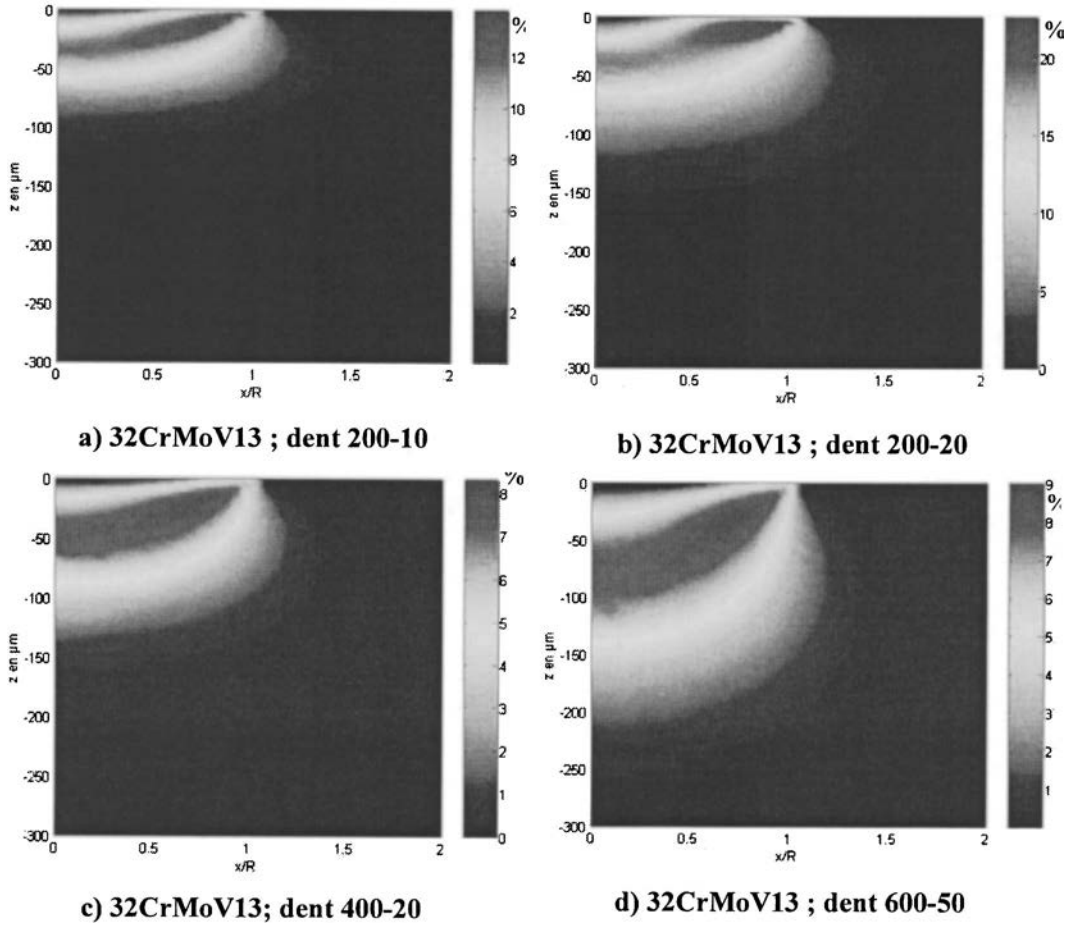

Fig. 16 Cumulated plastic strain introduced during indentation on nitrided 32CrMoV13 steel

(in micrometers) corresponds to the distance from the deformed surface. The horizontal (radial) axis is normalized by the dent radius. Results are presented for dents 200-10, 200-20, 400-20, and 600-50 carried out on 32CrMoV13 steel. The maximum equivalent plastic strain is found on dent 200-20 (20%). It is lower and ranges from 8 to 13% on the three remaining dents. The depth where plastic strain occurs is <150 μm in most cases (and always <250 μm). The maximum strain is found in the vicinity of $x/R=1$, close to the surface and drops steeply beyond this abscissa, i.e., when $x/R>1$.

Residual Stress. Figure 17 shows the residual stress field after unloading for the same dents from Fig. 16. First, very high Von Mises stresses are observed. These are always above 2000 MPa and up to 3000 MPa for dent 200-20. The maximum stress is found just above abscissa $x/R=1$, very close to the surface. Second, the stressed zone is not limited to the plastically deformed zone, but extends far away from it. For a surface point at abscissa $x/R=2$, the residual stress obtained is higher than 1000 MPa for all dents studied here.

To better understand the role of residual stresses produced by the indentation process, each term of the stress tensor should be considered as illustrated in Fig. 18 for dent 200-20. It can be concluded that the radial stress is essentially compressive within the first 150 μm. Conversely, terms $\sigma_{\theta\theta}$ and σ_{zz} are negative in the plastically deformed zone and positive elsewhere. Finally, the shear stress σ_{rz} is found maximum in the vicinity of the dent shoulder.

Indent Shape. Usually, the dent profile is approximated by the product of a cosine by a damping exponential function (Eq. (3)). In this relation only one parameter, K (the damping coefficient), is required to obtain the shoulder height

$$h(r) = h_p \cos\left(\frac{2\pi r}{4R}\right)\exp\left[-K\frac{r^2}{(4R)^2}\right] \tag{3}$$

Equation (3) has been plotted in Fig. 19 for the dent 200-20 and compared to those obtained by FE simulation of the nitrided material. It should be mentioned that the FEM simulation gives a dent profile that is globally close to the measured one. It is found that, while the dent depth, radius, and the height of its shoulder are well reproduced by Eq. (3), the shape of the dent is quite different from the FEM simulation (which is very close to the experimental profile).

For this reason a new function based on the previous one is proposed (Eq. (4)). It requires five parameters, h_p, R, I_1, I_2, and I_3. Within the dent ($r<R$), Eq. (3) is kept. Parameters I_1, I_2, and I_3 allow fitting the slope of the dent around the shoulder top and its location. The continuity of the function at $r=R$ is obtained by K, which depends on these five parameters. Figure 19 shows a good agreement between this analytical function and the FEM-simulated profile. Figure 20 presents the pressure distribution obtained using the analytical profile given by Eq. (3) and (4). It is found that Eq. (3) significantly underestimates the magnitude of the peak pressure obtained using the result of the FEM simulation or the equivalent geometry given by Eq. (4)

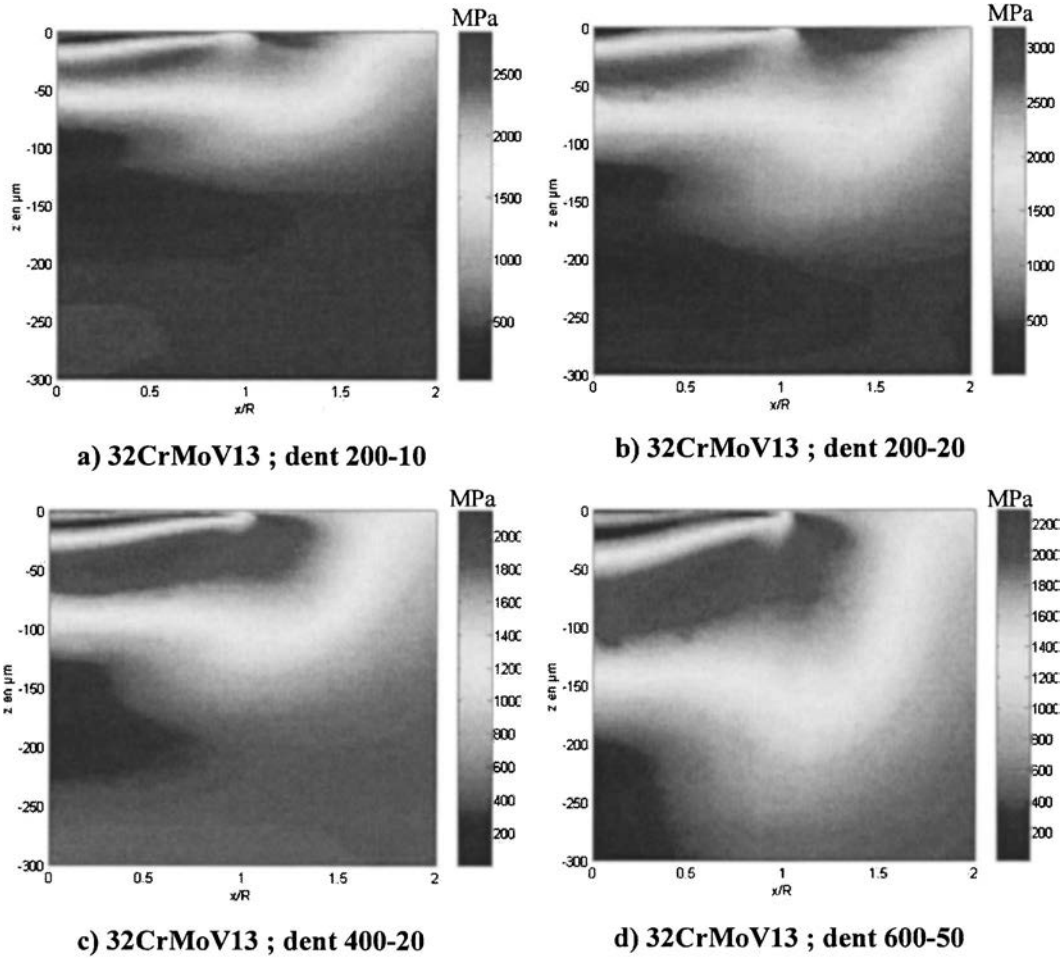

Fig. 17 Von Mises residual stress introduced during indentation on nitrided 32CrMoV13 steel

$$r < R$$

$$h(r) = h_p \cos\left(\frac{2\pi r}{4R}\right)\exp\left[-K\frac{r^2}{(4R)^2}\right] \quad \text{with}$$

$$K = -16\ln\left[\frac{2RI_1(I_3 - I_2)}{\pi h_p}\right]$$

$$r \geqslant R$$

$$h(r) = I_1\{\exp[-I_2(r-R)] - \exp[-I_3(r-R)]\} \tag{4}$$

Endurance Limit. The RCF endurance limit $H1$ is defined as the maximum contact pressure that a contact can bear without exceeding the microyield shear stress of the material [11]. For the present geometry, $H1$, which depends on the contact radius for a surface hardened material, is equal to 2.65 GPa for smooth (undented) nitrided 32CrMoV13 steel [14]. When the surface is dented, the local endurance limit $H1I$ is defined to account for local stresses around the dent. $H1I$ is the maximum load—expressed as the Hertz pressure of the equivalent smooth contact case—that can be sustained without locally exceeding the microyield shear stress in the vicinity of the dent.

In order to determine the endurance limit, only an elastic simulation of the overrolling of the dent is required. Residual stresses from nitriding and indentation are superimposed on the stresses due to contact. The total shear stress is subsequently calculated at each point and compared to the local microyield shear stress, which is modified by the work hardening that occurred during the indentation process. The contact problem is solved with a 3D contact code [18–21]. $H1I$ was calculated for every dent tested experimentally under pure rolling conditions. Dimensionless numerical results are presented in Fig. 21 for test $ES1$ (2.5 GPa, with no hoop stress). The numerical results are consistent with the experimental data. Each harmful dent exhibits an endurance limit $H1I$ lower than the applied contact pressure during test. This is consistent with the definition of the endurance limit.

Results given in Table 5 show the normalized endurance limit, $H1Id$ obtained by normalizing the endurance limit $H1I$ with a Hertz pressure higher than that normally encountered in aeronautical applications. $H1Id$ was investigated from 0.1 to 1. The lower bound was chosen since the contact zone becomes smaller than the dent. Dents are classified in three groups, low (L), medium (M), and high (H). Dents of group L have a very low $H1Id$ (<0.1). They undergo plastic deformation even under light loads and, consequently, are dangerous for most applications. Dents of group H have a very high $H1Id$. They are not dangerous in most pure rolling aeronautical applications. Last, group M is comprised of dents whose endurance limit $H1Id$ is between 0.1 and 1. Their harmfulness is application dependent.

When compared, these numerical results are consistent with the experimental data in Table 4. Figures 21–24 show dents sorted by increasing $H1Id$ along the vertical axis. For clarification, an arbitrary horizontal offset is applied. Numerical determination of $H1Id$ was made for pure rolling conditions without hoop stress. Figure 21 illustrates the behavior of dents for operating conditions $ES1$ using different symbols. A circle is assigned to harmful dents, a star for safe dents, and a square for dents with undetermined

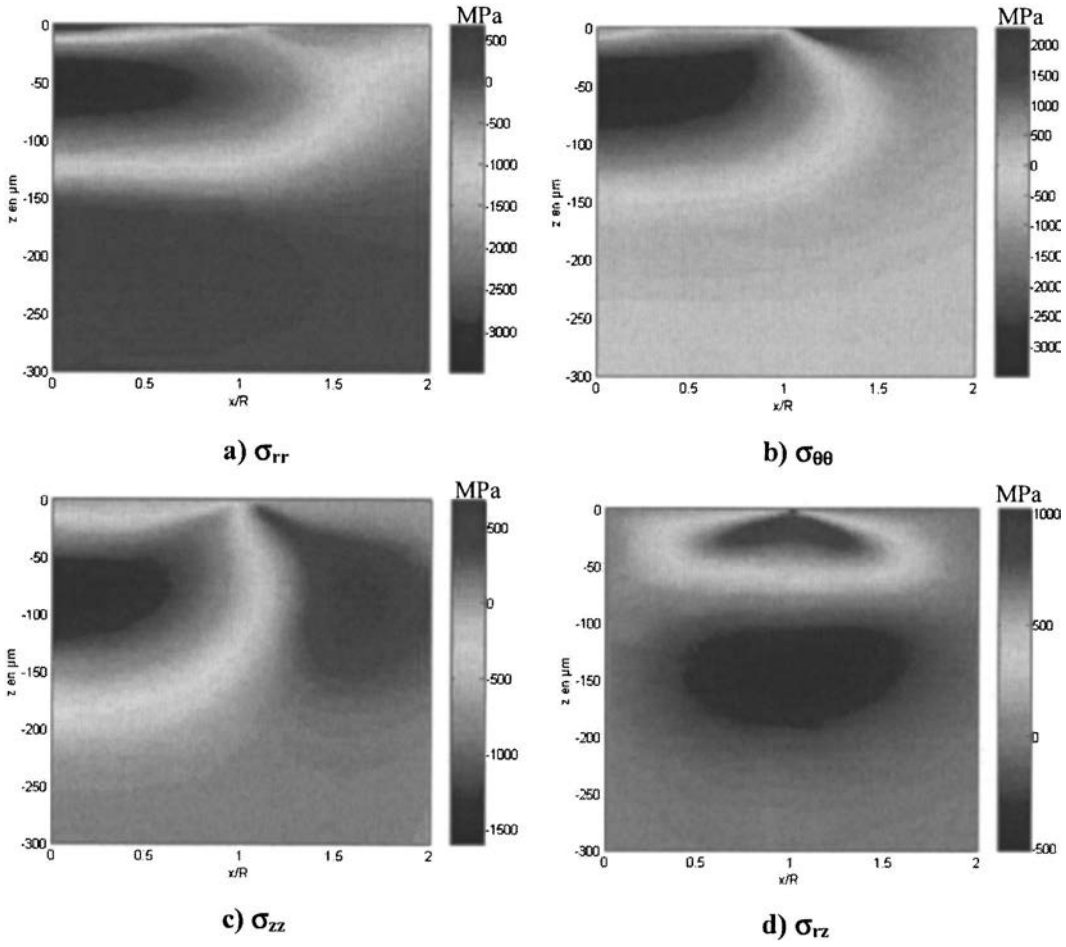

Fig. 18 Components of the residual stress tensor for dent 200-20 on nitrided 32CrMoV13 steel

behavior. Two major observations are made. First, dents whose *H*1*I* is higher than the applied load during test do not cause any damage. Second, all harmful dents have *H*1*I* lower than the applied load. Hence, using the predictions given by the *H*1*I* criteria, all harmful dents were identified and each dent that was assumed safe was effectively found to be safe. Therefore, *H*1*I* seems to be a valid definition of the local endurance limit.

The endurance limit *H*1*Id* was also determined for dents created on M50. The elastic plastic behavior of M50 was determined by Lamagnère et al. [22]. Results are compared for both steels in Figs. 22(*a*) and 22(*b*) for dents made with the indenter of radii R_p=200 and 400 μm at different loads W_i. For all dents, *H*1*Id* is experimentally equal or higher in nitrided 32CrMoV13 than in M50. In addition, materials are more efficiently discriminated with the R_p=400 μm indenter.

The effect of residual stress and hardening introduced during the indentation process were also studied. The endurance limit *H*1*Id* was determined for dents made on 32CrMoV13 steel surface in pure rolling, neglecting any residual stresses or hardening due to the indentation process. The results are labeled "geometry" in Fig. 23 and are based only on dent geometry and residual stresses due to nitriding. These results are compared to the real endurance limit, labeled "full" in the same figure. It is observed that residual stresses and hardening have an effect on the endurance limit and are not always protective, as often believed.

For artificially induced dents made with spherical diamond indenters, the variation of endurance limit *H*1*Id* with the average

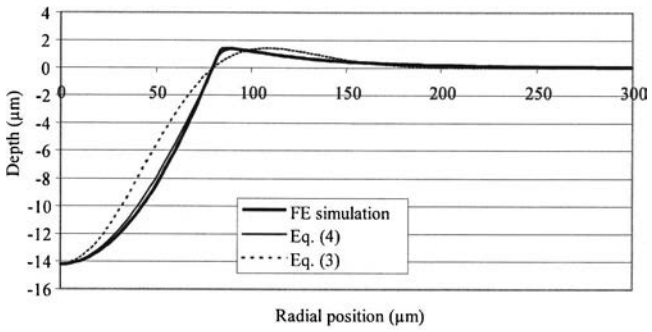

Fig. 19 Comparison of dent profiles obtained by FEM simulation for dent 200-20 (32CrMoV13) and by Eqs. (3) and (4)

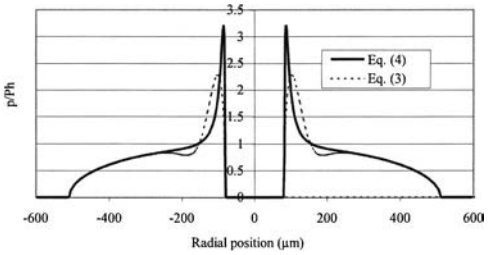

Fig. 20 Dimensionless pressure distribution, which results from dent profiles given in Eqs. (3) and (4)

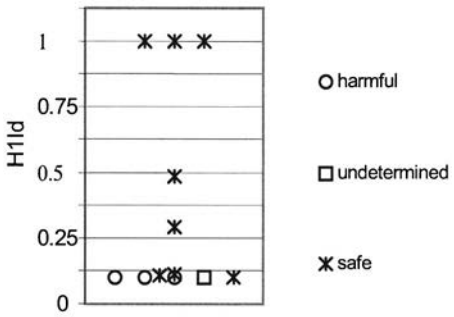

Fig. 21 Endurance limit *H1Id* found numerically for various dents in test *ES*1 versus experimental behavior

slope of the dent is monotonic, as seen in Fig. 24. If the elastic unloading is neglected during indentation and the diamond indenter is considered rigid, the dent is then a portion of a sphere and its average slope can be expressed by Eq. (5) below as a function of R, the radius of the dent and R_p, the radius of the indenter. During the indentation process, the contact pressure can be assumed constant as P_{ave} because of the load redistribution due to plastic deformation. The radius of the dent can then be related to the applied load W as given in Eq. (6). P_{ave} can be considered

Table 5 Dimensionless *H1Id* endurance limit in pure rolling conditions

Dent	H1Id	Dent	H1Id
200-5	0.107	400-20	0.112
200-10	< 0.1	400-50	< 0.1
200-20	< 0.1	600-5	> 1
200-50	< 0.1	600-10	> 1
400-5	> 1	600-20	0.485
400-10	0.292	600-50	< 0.1

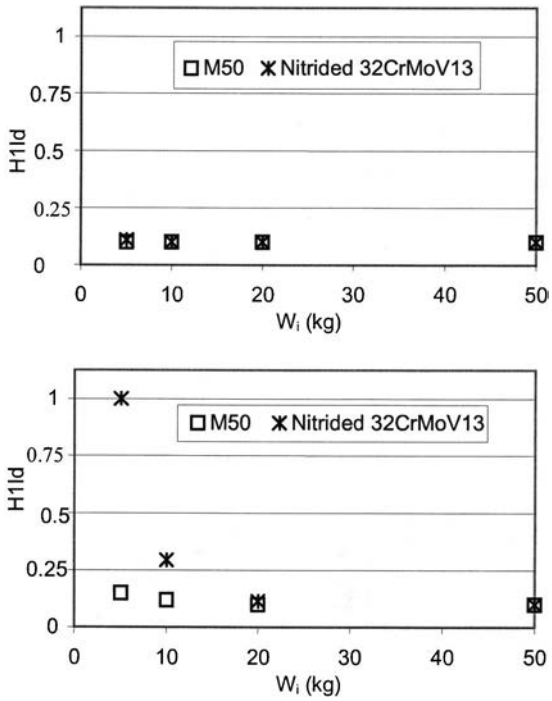

Fig. 22 Comparison of *H1Id* for nitrided 32CrMoV13 and M50: (*a*) R_p=200 μm and (*b*) R_p=400 μm

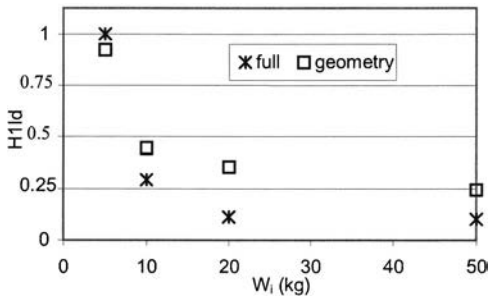

Fig. 23 Influence of hardening and residual stresses due to indentation on *H1Id*

constant for a given material also because of the asymptotic evolution of the stress-strain curve and the resulting large plastic deformation from indentation. Therefore, for a given material, the average slope of the dent evolves linearly with I_R, which is the ratio between the square root of the indentation load over the radius of the indenter (Eq. (7))

$$h_p = \frac{R^2}{2R_p} \tag{5}$$

$$R = \left(\frac{W}{\pi P_{ave}}\right)^{1/2} \tag{6}$$

$$p_m = \frac{h_p}{R} \approx \frac{W^{1/2}}{R_p} \tag{7}$$

Finally, dents can be sorted by increasing I_R. Experimental behavior of dents is reported in Fig. 25 for the given operating condition *ES*8. Two domains appear, harmful and safe. The transition between these two domains is noted as I_{Rlimit} and it depends on operating conditions. As far as dent initiated RCF is concerned, I_{Rlimit} can be considered as an indicator of the quality of the tested material for the given operating condition.

Conclusion

An original experimental procedure is proposed to discriminate the RCF live performance of bearing steels. It consists of denting the contacting surfaces by indenters with spherical tips of radii

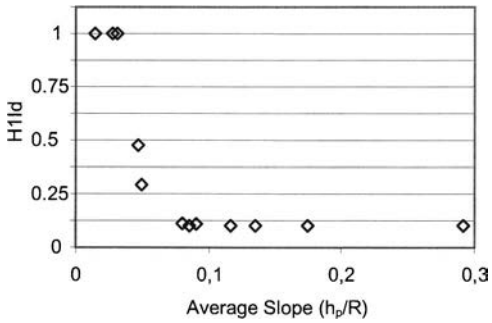

Fig. 24 Monotonic evolution of *H1Id* with the average slope of dents

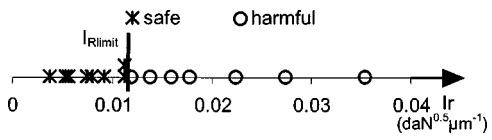

Fig. 25 I_R of dents and their experimental behavior for condition *ES*8

200, 400, and 600 μm with loads ranging from 5 to 50 daN. A new equation was derived to better describe the dent shapes. The following conclusions are drawn from fatigue tests performed on a high-speed twin-disk machine for disk specimens with artificial dents:

1. Nitrided 32CrMoV13 steel exhibits a better tolerance to surface dents when compared to conventional M50 bearing steel.
2. The applied normal load has a limited effect on the endurance limit.
3. Hoop stress has a slight effect on endurance limit within the domain investigated (0 and 115 MPa).
4. Sliding has a very detrimental effect on endurance limit.

The indentation process and the overrolling of dents was also simulated. A FEM analysis was performed to determine the plastic strain and residual stress fields due to indentation. A contact code was then used to study the overrolling of the load on the dent.

From these simulations, a physically based endurance limit criterion $H1I$ was calculated for various dents. The comparison of experimental data with numerical results shows that the $H1I$ criterion can be used to predict a lower bound of the local endurance limit.

This criterion was determined for identical dents made on nitrided 32CrMoV13 and M50 steels. Both experimental and numerical predictions show that nitrided 32CrMoV13 steel provides a significant improvement in dent initiated rolling contact fatigue resistance over M50.

For a given set of operating conditions and for dents made with a diamond spherical tip, the limit between safe and harmful dents can be represented in terms of $I_{R\text{limit}}$. This factor depends on operating conditions and material. For fixed operating conditions, $I_{R\text{limit}}$ could potentially represent the material response toward dent-initiated RCF.

Acknowledgments

Authors gratefully acknowledge Dr. Lewis Rosado of US Air Force for his critical reading of the manuscript.

Nomenclature

Notations

ϕ = dent diameter
τ_e = micro-yield shear stress
B, C, n = parameter of the Swift's law
E = Young's modulus of elasticity
f = friction coefficient in %
h = dent profile
h_b = height of dent shoulder
h_p = dent depth
I_1, I_2, I_3 = dimensionless parameters used in Eq. (4)
I_R = =W$^{0.5}$/R_p
K = damping coefficient for the dent geometry
P = pressure distribution
P_{ave} = average contact pressure during indentation
P_H = Hertz pressure (smooth contact)
p_m = =hp/R average slope of the dent
r = radial position (radius)
R = dent radius
R_{eq} = equivalent radius of the contacting bodies
R_p = indenter radius
W = contact load
W_i = indentation load
ε_p = equivalent plastic strain
υ = Poisson ratio
σ_{eq} = equivalent stress

Abbreviations

ARB = aeronautical rolling bearing
Dent *xxx-yy* = dent produced by a diamond indenter of radius R_p=*xxx* (in μm) under load W_i=*yy* (in daN)
FRIZ = friction and rolling initiation zone
$H1$ = endurance limit for a smooth contact, expressed in term of the Hertz pressure
$H1I$ = endurance limit for a dented surface, expressed in terms of the equivalent Hertz pressure
$H1Id$ = dimensionless endurance limit
RCF = rolling contact fatigue
RIZ = rolling initiation zone
TD = tested disk

References

[1] Tallian, T. E., 1992, *Failure Atlas for Hertz Contact Machine Elements*, ASME Press, New York.
[2] Nélias, D., and Ville, F., 2000, "Detrimental Effects of Dents on Rolling Contact Fatigue," ASME J. Tribol., **122**, pp. 55–64.
[3] El Ghazal, H., Lormand, G., Hamel, A., Girodin, D., and Vincent, A., 2001, "Microplasticity Characteristics Obtained Through Nano-indentation Measurements: Application to Surface Hardened Steels," Mater. Sci. Eng., A, **303**, pp. 110–119.
[4] Ghiglione, D., Leroux, C., and Tournier, C., 1996, "Pratique des Traitements Thermochimiques-Nitruration, Nitrocarburation et Dérivés," Techniques de l'ingénieur:MD, M 1222, pp. 1–44.
[5] Ko, C. N., and Ioannides, E., 1989, "Debris Denting—The Associated Residual Stresses and Their Effect on the Fatigue Life of Rolling Bearing: An FEM Analysis," *Proc. of 15th Leeds-Lyon Symp. on Tribology*, Leeds, England, 1988, D. Dowson et al., eds., Butterworths, pp. 199–207.
[6] Xu, G., and Sadeghi, F., 1996, "Spall Initiation and Propagation Due to Debris Denting," Wear, **201**, pp. 106–116.
[7] Xu, G., Sadeghi, F., and Cogdell, J. D., 1997, "Debris Denting Effects on Elastohydrodynamic Lubricated Contacts," ASME J. Tribol., **119**, pp. 579–587.
[8] Xu, G., Sadeghi, F., and Hoeprich, M. R., 1997, "Residual Stresses Due to Debris Effects in EHL Contacts," Tribol. Trans., **40**, pp. 613–620.
[9] Zhao, J., Sadeghi, F., and Nixon, H. M., 2000, "A Finite Element Analysis of Surface Pocket Effects in Hertzian Line Contact," ASME J. Tribol., **122**, pp. 47–54.
[10] Kang, Y. S., Sadeghi, F., and Hoeprich, M., 2004, "A Finite Element Model for Spherical Debris Denting in Heavily Loaded Contacts," ASME J. Tribol., **126**, pp. 71–80.
[11] Howell, M. B., Rubin, C. A., and Hahn, G. T., 2004, "The Effect of Dent Size on the Pressure Distribution and Failure Location in Dry Point Frictionless Rolling Contacts," ASME J. Tribol., **126**, pp. 413–421.
[12] Jacq, C., Lormand, G., Nélias, D., Girodin, D., and Vincent, A., 2003, "On the Influence of Residual Stresses in Determining the Micro-Yield Stress Profile in a Nitrided Steel by Nano-Indentation," Mater. Sci. Eng., A, **342**, pp. 311–319.
[13] Flamand, L., Berthe, D., and Godet, M., 1981, "Simulation of Hertzian Contacts Found in Spur Gears With a High Performance Disk Machine," ASME J. Mech. Des., **103**, pp. 204–209.
[14] Vincent, A., Fougères, R., Lormand, G., Dudragne, G., and Girodin, D., 2002, "Endurance Limit Model for Through Hardened and Surface Hardened Bearing Steels," in Bearing Steel Technology, ASTM STP 1419, pp. 459–473.
[15] Nélias, D., Dumont, M.-L., Couhier, F., Dudragne, G., and Flamand, L., 1998, "Experimental and Theoretical Investigation on Rolling Contact Fatigue of 52100 and M50 Steels Under EHL or Micro-EHL Conditions," ASME J. Tribol., **120**, pp. 184–190.
[16] Nélias, D., Dumont, M.-L., Champiot, F., Vincent, A., Girodin, D., Fougères, R., and Flamand, L., 1999, "Role of Inclusions, Surface Roughness and Operating Conditions on Rolling Contact Fatigue," ASME J. Tribol., **121**, pp. 240–251.
[17] Cercueil, H., 1999, "Etude d'une nouvelle nuance d'acier à roulement pour conditions d'usage sévères et modélisation de son endommagement en présence d'une indentation," Ph.D. thesis, INSA Lyon.
[18] Jacq, C., Nélias, D., Lormand, G., and Girodin, D., 2002, "Development of a Three-Dimensional Semi-Analytical Elastic-Plastic Contact Code," ASME J. Tribol., **124**, pp. 653–667.
[19] Sainsot, P., Jacq, C., and Nélias, D., 2002, "A Numerical Model for Elastoplastic Rough Contact," Comput. Model. Eng. Sci., **3**, pp. 497–506.
[20] Antaluca, C., Nélias, D., and Cretu, S., 2004, "A Three-Dimensional Friction Model for Elastic-Plastic Contact With Tangential Loading—Application to Dented Surfaces," *Proc. of 2004 ASME/STLE Int. Joint Tribology Conference*, ASME, New York, ASME Paper No. TRIB2004-64331.
[21] Boucly, V., Nélias, D., Liu, S., Wang, Q. J., and Keer, L. M., 2005, "Contact Analyses for Bodies With Frictional Heating and Plastic Behavior," ASME J. Tribol., **127**, pp. 355–364.
[22] Lamagnère, P., Fougères, R., Lormand, G., Vincent, A., Girodin, D., Dudragne, G., and Vergne, F., 1998, "A Physically Based Model for Endurance Limit of Bearing Steels," ASME J. Tribol., **120**, pp. 421–426.